Urban Climate 49 (2023) 101527

Contents lists available at ScienceDirect

Urban Climate

journal homepage: www.elsevier.com/locate/uclim

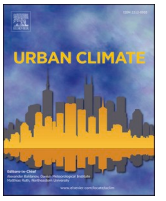

# Assessing the performance of the non-hydrostatic RegCM4 with the improved urban parameterization over southeastern China

Thanh Nguyen-Xuan [a,b], Eun-Soon Im [a,c,*]

[a] Division of Environment and Sustainability, The Hong Kong University of Science and Technology, Hong Kong, China
[b] University of Science and Technology of Hanoi, Vietnam Academy of Science and Technology, Viet Nam
[c] Department of Civil and Environmental Engineering, The Hong Kong University of Science and Technology, Hong Kong, China

ARTICLE INFO

*Keywords:*
Non-hydrostatic RegCM4
Building energy model
Pearl River Delta
Yangtze River Delta

ABSTRACT

This study evaluates the performance of the non-hydrostatic RegCM4 model (RegCM4-NH) incorporating the building energy model (BEM) in simulating urban climate over the Pearl River Delta (PRD) and Yangtze River Delta (YRD) regions. Specifically, it focuses on examining how the inclusion of BEM can ameliorate the severe warm bias in urban grids observed in high-resolution RegCM4 simulations by improving the surface energy balance. The prognostic calculation of interior building temperature and the consideration of ventilation and heat transfer between the building and the environment can collectively lead to a better estimate of anthropogenic heat flux (AHF). The effect of BEM does not appear to be uniform, showing spatial and temporal variations. While the magnitude of AHF reduction is roughly proportional to the urban density, the maximum reduction occurs at nighttime, which results in an asymmetric response to the minimum and maximum temperatures. Although the degree of lowering temperature is not sufficient to remove the systematic warm bias, adding physical realism to the model is helpful to make further improvements. The performance evaluation of RegCM4-NH with BEM targeted in vast urban agglomerations for the first time will be a valuable reference to facilitate the wider use of RegCM4-NH in the study of urban surface impacts.

## 1. Introduction

According to the United Nations, Department of Economic and Social Affairs, Population Division (2018), the percentage of the world's urban population increased from 30% in 1950 to 55% in 2018 and is estimated to touch 68% by 2050. China is among the fastest urban population-growing countries. In particular, the Pearl River Delta (PRD, including Guangzhou, Shenzhen, and Hong Kong) and the Yangtze River Delta (YRD, including Shanghai and Nanjing) are considered among the largest urban agglomerations in China. Apart from witnessing the ongoing fast-faced urbanization, these regions are also expected to be highly vulnerable to anthropogenic warming (Zhang et al., 2016; Yang et al., 2019; Qing and Wang, 2021; Wang et al., 2021). Importantly, the urban expansion may deteriorate the negative impacts of extreme heat waves across areas where the heat stress has already often exceeded a dangerous level in summer. Therefore, it is paramount to quantify the effect of urban heat island (UHI) on thermal discomfort in current and future climate conditions.

* Corresponding author at: The Hong Kong University of Science and Technology, Academic Building 4602, Clear Water Bay, Kowloon, Hong Kong, China.
*E-mail address:* ceim@ust.hk (E.-S. Im).

https://doi.org/10.1016/j.uclim.2023.101527
Received 7 February 2022; Received in revised form 20 March 2023; Accepted 14 April 2023
Available online 3 May 2023

Notably, the regional climate model (RCM) can be a useful tool to ascertain the modifications of surface-atmosphere exchanges of heat, moisture, and momentum owing to land-use/land-cover changes. If the cropland is converted into urban, the land surface scheme embedded in RCM modifies not only the dominant surface properties (e.g., surface albedo, roughness length, displacement height, surface emissivity, heat capacity, thermal conductivity) but also the relevant physical processes related to surface energy partitioning and the water cycle (Grimmond et al., 2009). Very high-resolution RCM simulations at convection-permitting grid spacing (e.g., a few kilometers) are particularly required to investigate the effect of urbanization on regional climate due to the localized nature of urban extent. Studies modeling urban effects using RCMs are eliciting a great deal of attention in China, with most modeling studies being conducted using the Weather Research and Forecasting (WRF) model (Chen et al., 2011; Wang et al., 2012; Yan et al., 2016; Li et al., 2017; Zhao and Wu, 2017; Dai et al., 2019; Xiao et al., 2019; Yang et al., 2019; Kwok and Ng, 2021; Wang et al., 2021, Wong et al., 2021). While the International Centre for Theoretical Physics (ICTP) regional climate model version 4 (RegCM4) has been extensively used for climate simulations to a grid spacing of up to 10 km (Giorgi et al., 2012), its utilization to examine the impact of urbanization has been rather limited so far. This is attributed to the fact that the urban module is not actively working with a relatively coarse resolution under the hydrostatic dynamical core. However, given that the non-hydrostatic RegCM4 (RegCM4-NH) has been released recently, the convection-permitting simulations or urbanization simulations have started being conducted across the European region (e.g., Coppola et al., 2020; Pichelli et al., 2021; Ban et al., 2021; Huszar et al., 2020a & b). Subsequently, in what is viewed as the first attempt to evaluate the performance of RegCM4-NH over monsoon-dominated regions of East Asia, Nguyen-Xuan et al. (2021) evaluated the performance of RegCM4-NH at 4 km grid spacing over the PRD and YRD urban regions and demonstrated the great potential of RegCM4-NH in simulating the fine-scale climate characteristics over the targeted regions. According to this study conducted by Nguyen-Xuan et al. (2021), the performance of RegCM4-NH is comparable to the convection-permitting WRF simulations over the PRD and YRD regions.

In the present study, we investigate the urbanization effects on the climate characteristics over the PRD and the YRD regions utilizing the RegCM4-NH model with the same configuration used in Nguyen-Xuan et al. (2021), albeit with an improved urban module. For the RegCM4 simulations, the so-called CLMU (Oleson et al., 2008a, 2008b), which is the default urban canopy module incorporated into the Community Land Model version 4.5 (CLM4.5, Oleson and Lawrence, 2013), is used to resolve the bio-physical processes associated with the urbanized surface. The transferability and sensitivity of CLMU within RegCM4 have been tested in areas of Europe (Halenka et al., 2019; Karlický et al., 2018; Huszar et al., 2020a, 2020b; Karlický et al., 2020). Based on these previous studies, the default version of CLMU tends to markedly overestimate temperature over the urban grids and the magnitude of overestimation becomes larger as the resolution increases. For example, Huszar et al. (2020a) demonstrated using RegCM4 with CLMU that the nested domain at 3 km resolution overestimates temperature against observation, even though its parent domains with 27 km and 9 km grid spacing cause the negative bias. Huszar et al. (2020b) also reported that the simulation at 1 km resolution shows significant overestimation during nighttime. On the other hand, Oleson and Feddema (2020) reported that the deficiency of CLMU could be attributed to two possible reasons. Firstly, the unrealistic prescription of urban properties (i.e., the building morphology, radiative and thermal characteristics of road and building roof and walls, and the settings of interior temperature for heating and air conditioning) can enhance the heat transfer between the exterior and interior of a building. Secondly, the curtailed accuracy in the calculation of interior building temperatures may lead to the excessive release of anthropogenic heat flux (AHF). In order to help ameliorate this problem, a building energy model (BEM) similar to the one developed by Bueno et al. (2012) has been incorporated into the recent version of CLM5 with some simplifications to suitably operate for long-term high-resolution simulations (Oleson and Feddema, 2020). In contrast to the original CLMU, incorporating BEM into CLMU allows the land surface model to treat the interior building temperature as a prognostic variable updating every time step, which, in turn, results in better estimates of AHF release into the atmosphere. The accurate estimation of AHF is proven to be very important, in particular for the future projection of urban climate (Doan et al., 2019).

In this regard, we have incorporated the BEM of CLM5 with updated urban properties (Oleson and Feddema, 2020) into CLM4.5 embedded in RegCM4-NH to alleviate the well-known problem of temperature overestimation in urban grids. Currently, RegCM4-NH is set up to enable CLMU to perform for only those grid points where the urban fraction is higher than 40%. Neglecting the low-to-medium density urban may make the CLMU's deficiency appear less apparent, but it cannot be considered the fundamental solution. It is worth mentioning that very high urban density (e.g., tall building district) usually appears with a small fraction (as shown in Fig. S1) but may introduce great effects. Therefore, it is necessary to remove or reduce the current 40% threshold (even 80% in some earlier versions) in RegCM4 in order to comprehensively simulate urban impacts at different density classes. The first focus of this study is placed on investigating whether the physical realism added by the BEM is capable of improving the performance of RegCM4-NH simulations over the PRD and YRD regions. Then, a comparative assessment of the characteristics of urban heat island (UHI) between the PRD and YRD regions is carried out. Although both PRD and YRD have experienced rapid urbanization over the past few decades, the effect of UHI may emerge differently through the interaction with meteorological backgrounds in these regions. This study could serve as a prerequisite before conducting future projections that consider the temporal evolution of urban growth under different levels of global warming. In addition, this study will serve as a valuable reference to foster the usage of the RegCM4-NH model for urban climate studies across other regions.

## 2. Model configuration and experimental design

### 2.1. Non-hydrostatic RegCM4 and domain configuration

The Regional Climate Model version 4.7 with the non-hydrostatic dynamical core (Coppola et al., 2021) is used for simulating the

regional climate over the PRD and YRD regions. Fig. 1 illustrates the domain setting with one parent domain and two nested domains along with their respective topography and urban density. The parent domain (hereafter referred to as D1) encompasses most parts of southeastern China along with adjacent countries (e.g., Korea, Japan) with a horizontal resolution of 20 km. On the other hand, the two nested domains (hereafter referred to as D2) focus on the PRD and YRD regions with a horizontal resolution of 4 km. The comparison of spatial distributions between topography and urban density clearly demonstrates that high urban density mostly appears in low-lying areas below 100 m elevation above sea level. Urban density comprises the sum of three urban classes: tall building district (TBD, i.e., very high density), high density (HD), and medium density (MD) (Fig. S1). The geographic extent of TBD appearing in Fig. S1 (a) is in consonance with the location of high urban density above 40% shown in Fig. 1 (d, e). For the vertical resolution, the D1 and two D2 simulations employ 23 and 41 levels, respectively. The D1 simulation is driven by the initial and lateral boundary conditions from the ERA-Interim reanalysis with a resolution of $0.75^\circ \times 0.75^\circ$ at 6-h intervals (Dee et al., 2011). All simulations are integrated between 01 May and 01 September for each year of the 2000–2009 decade. The first month of each year's simulation (i.e., May) is considered to be a spin-up period and thus discarded from the analysis. For each D2 domain, two simulations are performed with the default CLMU and the BEM newly added to CLMU. Table 1 summarizes additional details of individual simulations.

The non-hydrostatic dynamical core (Coppola et al., 2021) and convective parameterization from Emanuel (Emanuel and Živković-Rothman, 1999) are used for all simulations. It is noteworthy that 4 km is within the 'gray-zone resolution', wherein deep convection is partly resolved and partly sub-grid. When performing the sensitivity tests of convective parameterization turn-on/off, we found that the Emanuel scheme performs better in comparison to the convection-permitting simulation (Nguyen-Xuan et al., 2021). The land surface processes are modeled with CLM4.5 (Oleson and Lawrence, 2013), and the urban module turns on for only two nested domains.

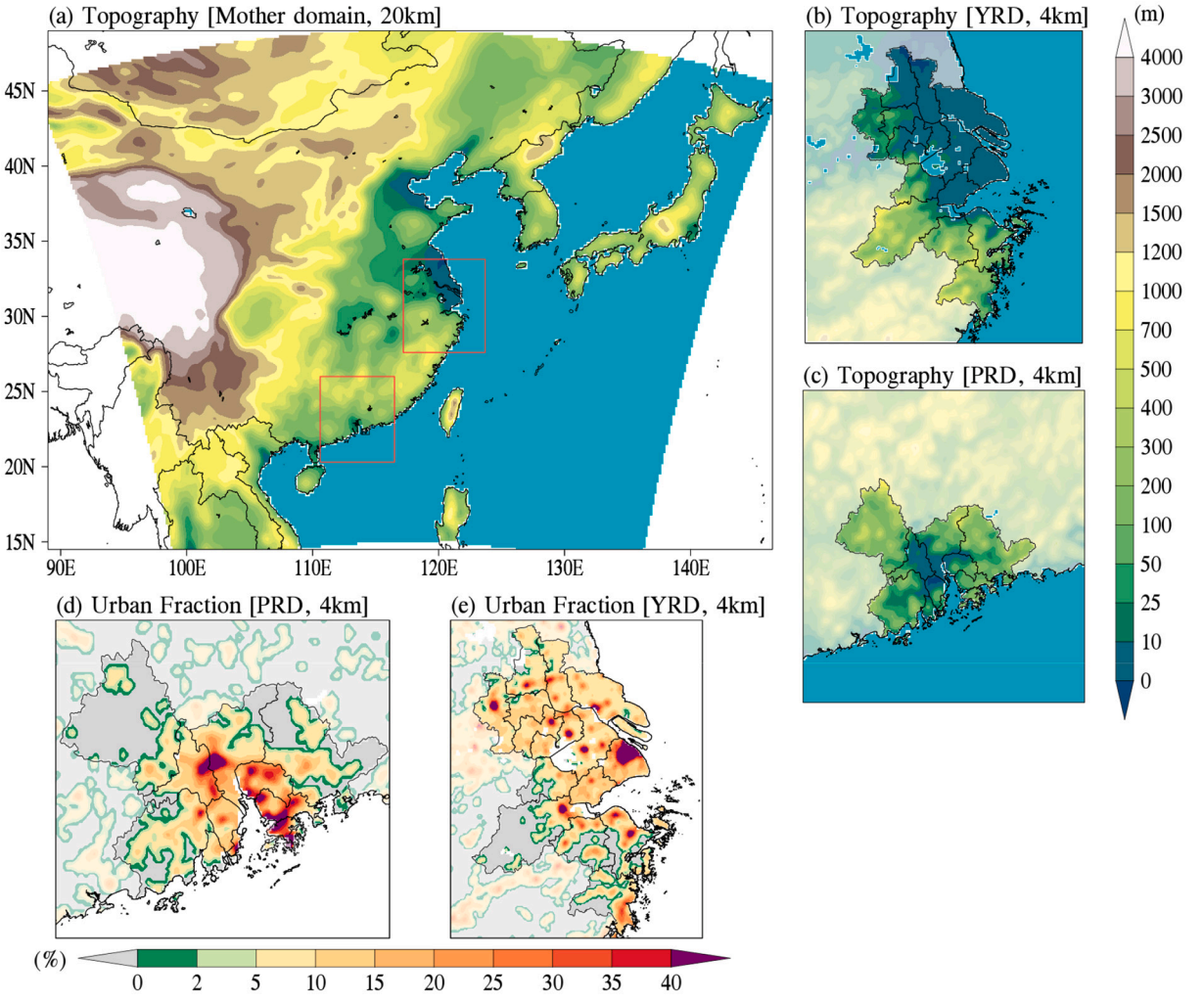


**Fig. 1.** Domain and topography (unit: m) used for the parent domain (a) and two nested domains (b, c) simulations. The geographical locations of two nested domains are marked by red rectangles in panel (a). The Pearl River Delta (PRD) and Yangtze River Delta (YRD) focused in this study are shown respectively in panel (d) and (e) with the distribution of urban fraction (unit: %) used in CLMU. (For interpretation of the references to colour in this figure legend, the reader is referred to the web version of this article.)

**Table 1**
Summary of experimental design and RegCM4 configuration.

| Exp. Name | Area | Resolution | Dimension (lon×lat×lev) | Urban | Shared Configuration |
|---|---|---|---|---|---|
| D1 | East Asia | 20 km | 225 × 195 × 23 | Off | Non-hydrostatic core |
| D2-PRD-Def | PRD | 4 km | 161 × 161 × 41 | Default | CPS: Emanuel |
| D2-PRD-BEM | PRD | 4 km | 161 × 161 × 41 | BEM | Microphysics: SUBEX |
| D2-YRD-Def | YRD | 4 km | 161 × 181 × 41 | Default | PBL: Holtslag<br>Land surface: CLM4.5 |
| D2-YRD-BEM | YRD | 4 km | 161 × 181 × 41 | BEM | Radiation: CCM3<br>Ocean flux: Zeng |

Other configurations include the microphysics from the Subgrid Explicit Moisture Scheme (SUBEX, Pal et al., 2000), the planetary boundary layer parameterization based on Holtslag et al. (1990), the radiative transfer scheme from the National Center for Atmospheric Research (NCAR) Community Climate Model version 3 (CCM3, Kiehl et al., 1998), and the ocean flux scheme from Zeng et al. (1998). These physical parameterizations are identical to those adopted in Nguyen-Xuan et al. (2021), with the exception of implementing BEM to CLM4.5.

### 2.2. Urban parameterization in CLM4.5

In RegCM4, the land-surface processes and their interactions with the atmosphere are represented by the CLM4.5 which uses the subgrid hierarchy based on the mosaic approach. This method allows the model to proportionally include all types of land use as well as to simulate simultaneously all possible related processes at each grid point. The urban processes are simulated by a sub-model, also

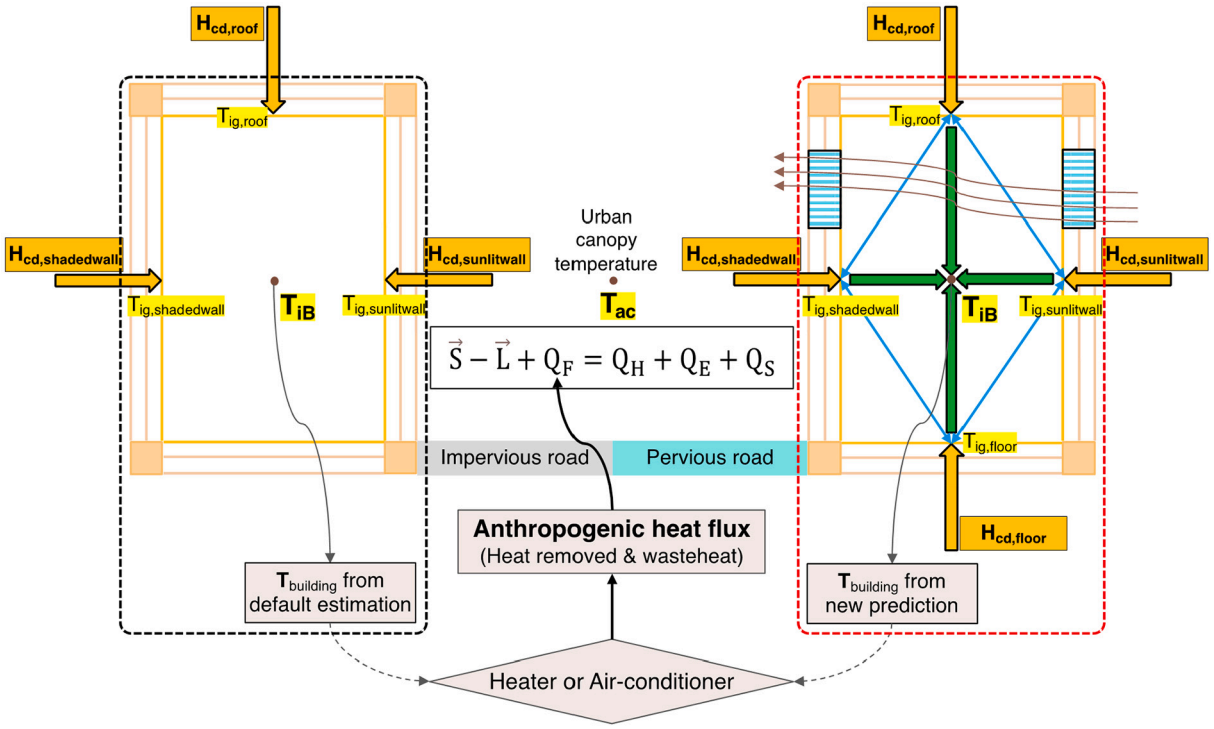


**Fig. 2.** Schematic diagram for the comparison between default CLMU (marked by black-dashed line) and BEM newly added into CLMU (marked by red-dashed line) in estimating the interior building air temperature ($T_{iB}$), which is used to calculate the amount of anthropogenic heat flux ($Q_F$) contributed from the building to urban canyon due to heating and air-conditioning activities. The building is composed by "surfaces" including roof, sunlit wall, shaded wall, and floor. The urban canopy air temperature ($T_{ac}$) affects $T_{iB}$ by transferring the heat into the building by the conductions ($H_{cd,surfaces}$) through roof, sunlit wall, and shaded wall and forming the temperature at the inner most layer of each surface ($T_{ig,roof}$, $T_{ig,sunlitwall}$, $T_{ig,shadedwall}$). While the default CLMU estimates $T_{iB}$ based on a simple weighted average of roof, sunlit wall, and shaded wall temperatures, the BEM calculates $T_{iB}$ prognostically as a result of the balance between conduction (orange arrows), convection (green arrows), and radiation (blue arrows) on each surface and with the ventilation (curved arrows through the windows). The BEM also takes into account the balance on floor surface where the heat can be transferred between building and ground based on floor temperature ($T_{ig,floor}$). (For interpretation of the references to colour in this figure legend, the reader is referred to the web version of this article.)

known as CLMU, which is a single-layer urban canopy model developed by Oleson et al. (2008a & b). CLMU considers the urbanized surface to be a classical canyon representation of urban geometry described by building height (H) and street width (W) and composed of the roof, sunlit wall, shaded wall, pervious surface (e.g., residential lawns and parks), and impervious surface (e.g., roads, parking lots, sidewalks). In an urban canyon, the trapping of solar radiation ($\overrightarrow{S}$), longwave radiation ($\overrightarrow{L}$), and the surface-atmosphere exchanges of heat, mass as well as momentum are modulated by the properties of each urban density type, such as the materials of roads and building surfaces, the morphology of the urban environment, and human behaviors. In CLMU, these processes are described under the fundamental balance of net radiation ($\overrightarrow{S} - \overrightarrow{L}$), AHF from building space heating and air conditioning ($Q_F$), and the sum of the turbulent sensible and latent heat fluxes ($Q_H + Q_E$) in addition to net storage heat fluxes ($Q_S$) for each urban surface:

$$\overrightarrow{S} - \overrightarrow{L} + Q_F = Q_H + Q_E + Q_S \quad (1)$$

The net radiation ($\overrightarrow{S} - \overrightarrow{L}$) is computed from the downward shortwave ($S_\downarrow$) and longwave radiation ($L_\downarrow$) and the upward shortwave ($S_\uparrow$) and longwave ($L_\uparrow$) radiation (i.e., $S_\downarrow - S_\uparrow + L_\downarrow - L_\uparrow$). $Q_H$, and $Q_E$, are derived from the Monin-Obukhov similarity theory while $Q_S$ is the residual term in Eq. (1). CLMU is designed to simulate for multiple density classes (i.e., MD, HD, TBD in Fig. S1) appearing in each grid cell, instead of considering only the most dominant class as in previous versions. Due to its simplicity and computational efficiency, CLMU is beneficiated to long-term climate simulations at high resolution. Indeed, CLMU has been widely applied for the simulations of urban climate impacts and was ranked in the upper third of the 32 urban model intercomparison project (Grimmond et al., 2011; Oleson and Feddema, 2020).

### 2.3. Implementation of BEM to CLMU

In previous studies, the overestimation of AHF in CLMU has been recognized and two possible reasons have been addressed (Oleson and Feddema, 2020). First, the thermal properties of the roof and walls and their descriptions for thermal conductivity may remain unrealistic, thereby resulting in an improper amount of heat transfer between the exterior and interior of the building, which, in turn, can sequentially affect the estimation of the AHF. Second, the process of calculating the interior building air temperature ($T_{iB}$) seems to be too simplistic, just taking the weighted average of the interior roof and wall surface temperatures (Oleson, 2012). As shown in Fig. 2, urban canopy air temperature ($T_{ac}$) affects the temperature in the innermost layer of each surface ($T_{surfaces}$) of the building by heat conduction ($H_{cd,surfaces}$) through the roof and walls. For the default CLMU (marked by a black-dashed line in Fig. 2), $T_{iB}$ is only determined by the heat conduction through building surfaces (roof, shaded wall, and sunlit wall). No heat transfer takes place from the bottom layer and there is no natural heat transfer by ventilation as well. On the other hand, the implementation of BEM enables the inclusion of more components that directly affect $T_{iB}$ (marked by red-dashed line in Fig. 2). More specifically, the interior surface temperature of each surface (i.e., $T_{ig,roof}$, $T_{ig,shadedwall}$, $T_{ig,sunlitwall}$, and $T_{ig,floor}$ in Fig. 2) can be calculated using Eq. (2) that represents the energy balance of heat conduction ($F_{cd}$), convection ($F_{cv}$), and radiation ($F_{rd}$) for each interior surface (i.e., roof, shaded wall, sunlit

**Table 2**
Parameters used in the BEM and the urban properties over PRD and YRD.

| BEM parameters | Units | Value |
|---|---|---|
| Air changes per hour | $hr^{-1}$ | 0.3 |
| Convective heat transfer coefficient | $Wm^{-2}\,K^{-1}$ | 0.948–4.040 |
| Emissivity of interior surfaces | – | 0.9 |
| Floor thickness | m | 0.1 |

| Urban properties | Units | TBD | HD | MD |
|---|---|---|---|---|
| Canyon height to weight ratio | – | 7.2 | 1.8 | 0.48 |
| Height of roof | m | 180 | 45 | 12 |
| Fraction of roof | – | 0.5 | 0.6 | 0.35 |
| Roof thickness | m | 0.26 | 0.15 | 0.15 |
| Wall thickness | m | 0.32 | 0.29 | 0.29 |
| Roof type | – | BUR/concrete_deck | BUR/wood_deck | BUR/wood_deck |
| Wall type | – | conc_panel/ conc_masonry | brick_veneer/ conc_masonry | brick_veneer/ conc_masonry |
| Road type | – | concrete_road/ conc_masonry | asphalt_road/ stabilized | asphalt_road/ stabilized |
| Emissivity of roof | – | 0.91 | 0.92 | 0.92 |
| Emissivity of wall | – | 0.9 | 0.9 | 0.9 |
| Emissivity of pervious road | – | 0.95 | 0.95 | 0.95 |
| Emissivity of impervious road | – | 0.88 | 0.91 | 0.91 |
| Minimum internal building temperature | °C | 19 | 12 | 12 |
| Maximum internal building temperature | °C | 27 | 37 | 37 |

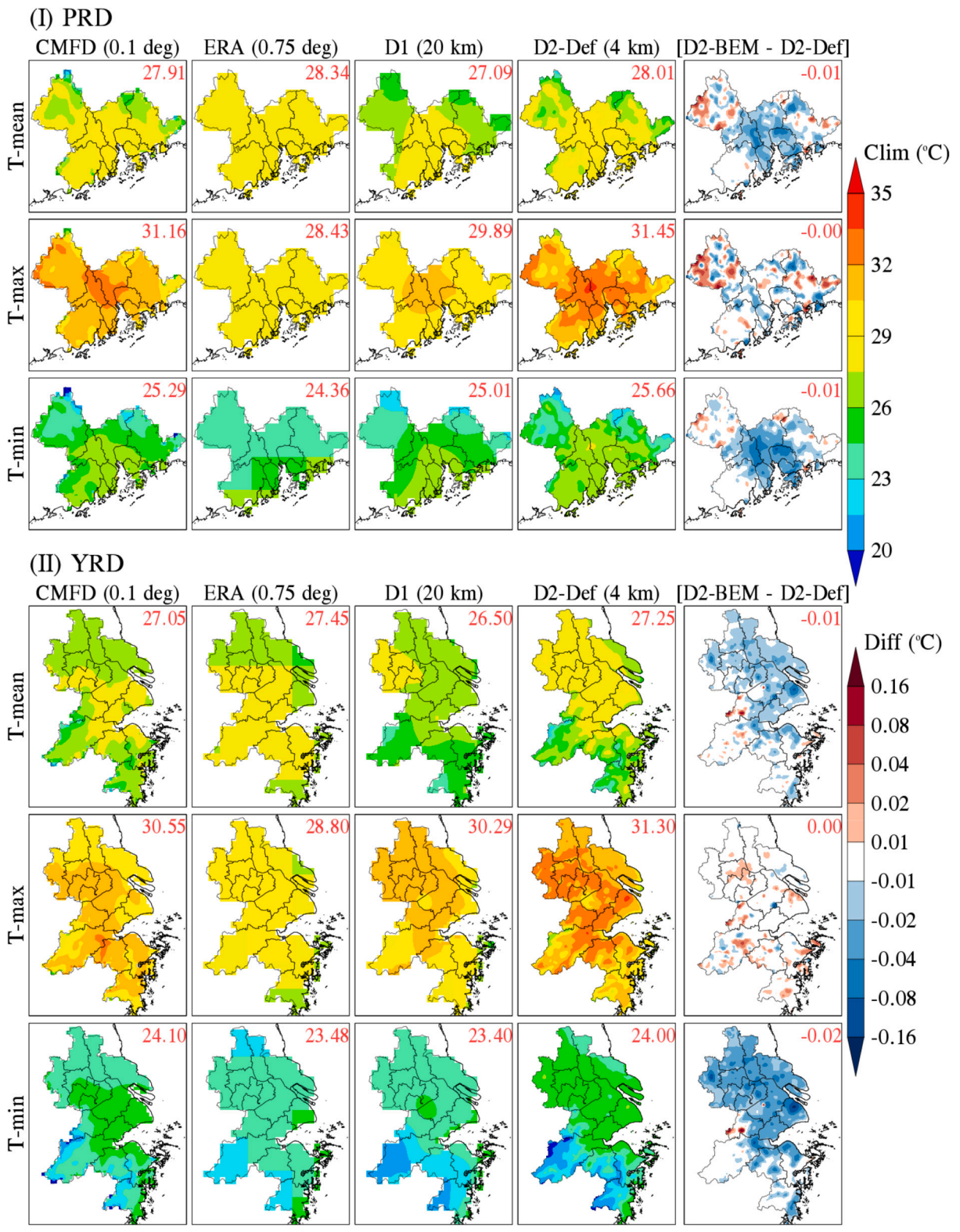


(caption on next page)

**Fig. 3.** The spatial distribution of 10-year average (2000–2009) JJA mean temperature (T-mean), maximum temperature (T-max), and minimum temperature (T-min) from CMFD observation, Era-Interim (ERA) reanalysis, parent domain simulation (D1), nested domain simulation with default CLMU (D2-Def), and its difference from nested domain simulation with BEM (D2-BEM minus D2-Def) over PRD (I) and YRD (II). The red number in the top-right corner denotes the area-average value (unit: °C). (For interpretation of the references to colour in this figure legend, the reader is referred to the web version of this article.)

wall, and floor). Here, since the subscript of "sfc" indicates all four surfaces collectively, Eq. (2) can be expanded to four and each one is used to calculate $T_{ig,roof}$, $T_{ig,shadedwall}$, $T_{ig,sunlitwall}$, and $T_{ig,floor}$, respectively.

$T_{iB}$ is then determined by the balance of heat fluxes on building air after taking ventilation into consideration as described in Eq. (3). The inclusion of the heat transfer between the building and the ground through the floor makes it possible to lower $T_{iB}$ during nighttime while its effect on $T_{iB}$ during the daytime may depend on the environmental conditions. This is because the $T_{ac}$ is usually higher/lower than the $T_{iB}$ during the day−/night-times. Meanwhile, the heat can be transferred in and out of the building along with the ventilation rate, thus leading to an increase/decrease in $T_{iB}$. These processes, which are only taken into consideration in BEM, but not in default CLMU, are expected to enhance the accuracy of $T_{iB}$, subsequently controlling the amount of the release of AHF that contributes to the energy balance in the urban canopy. In addition, the equations enable the BEM to prognostically predict $T_{iB}$ at every time step, expecting more realistic temporal variations.

$$F_{cd,sfc} + F_{cv,sfc} + F_{rd,sfc} = 0 \tag{2}$$

$$V_B \rho C_P \frac{\partial T_{iB}}{\partial t} - \sum_{sfc} A_{sfc} h_{cv,sfc} \left(T_{ig,sfc} - T_{iB}\right) - \dot{V}_{vent} \rho C_P (T_{ac} - T_{iB}) = 0 \tag{3}$$

The parameters in Eq. (3) include the following: $V_B$ refers to the volume of building air, $\rho$ is the density of dry air at standard pressure, $C_P$ signifies the specific heat of dry air, $A_{sfc}$ denotes the area of the surface, $h_{cv,sfc}$ and $T_{ig,sfc}$ signify the convective heat transfer coefficient and interior surface temperature at each surface (i.e., $T_{ig,roof}$, $T_{ig,shadedwall}$, $T_{ig,sunlitwall}$, and $T_{ig,floor}$), and $\dot{V}_{vent}$ is a constant for the ventilation air flow rate. Once the calculation of $T_{iB}$ is completed at the given time step, the AHF is estimated in the same way as the default CLMU (Oleson and Feddema, 2020). Specifically, the maximum/minimum internal building temperatures prescribed as the thermostat of the building (Table 2) are used to control the need for heating and air conditioning, which can determine the amount of AHF released. As a case in point, when the $T_{iB}$ is higher/lower than the prescribed maximum/minimum internal building temperature, the AC/heater will be activated to cool down/warm up the building. Then, the energy required to decrease or increase $T_{iB}$ is converted to sensible heat to calculate the AHF released into the climate system. More details can be found in Oleson and Feddema (2020).

### 2.4. Updated urban dataset and observational data for validation

Apart from the implementation of BEM to RegCM4-NH, all of our simulations are performed with the updated urban distribution and properties provided by Oleson and Feddema (2020), whereas the previous studies based on default CLMU use the urban dataset provided by Jackson et al. (2010). The updated dataset includes the spatial distribution in the percentage of three urban density classes, including TBD, HD, and MD, for each 1 km resolution grid cell. The buildings' morphological, thermal, and radiative characteristics as well as building interior maximum and minimum thermostat settings are grouped into 33 geographic regions where both social and physical characteristics are similar. This dataset was collected and converted to be suitably used in CLMU through the utilization of the Toolbox for Human-Earth System Integration & Scaling (THESIS) tool set (Feddema and Kauffman, 2016; Oleson and Feddema, 2020). Oleson and Feddema (2020) reported that an updated dataset for urban properties has been reduced to the global average temperature of 0.02 °C from the global simulation using the Community Earth System Model (CESM). One limitation of using this data for our study is that both PRD and YRD share the same urban properties because China, in its entirety, is now considered to be one of the 33 regions. Table 2 provides the parameters used in the BEM and urban properties corresponding to the three urban density types used in CLMU.

The 3-hourly near-surface temperature is obtained from China Meteorological Forcing Dataset (CMFD) with a grid spacing of 0.1-degree (Yang and He, 2019; He et al., 2020). The CMFD was produced from the combination of remote sensing products, reanalysis data, and in-situ station observations. Furthermore, daily mean, maximum, and minimum temperatures from ERA-Interim reanalysis data with a resolution of 0.75° × 0.75° are also compared with simulations for reference.

## 3. Results

### 3.1. Validation of the improvement from the implementation of BEM

We begin our analysis with the 10-year summer climatological patterns of the daily mean (Tmean), maximum (Tmax), and minimum (Tmin) temperatures over the PRD and YRD regions (Fig. 3). The temperatures from the D2 simulation with default CLMU are compared with those from CMFD observations and ERA-Interim reanalysis data as well as D1 simulation. The temperatures from ERA-Interim completely miss the spatial variability owing to its coarse resolution. On the other hand, D1 simulation driven by ERA-Interim reanalysis produces temperatures that are much closer to the CMFD observations. Therefore, the dynamical downscaling of ERA-Interim reanalysis data using RegCM4-NH is capable of bringing quantitative and qualitative improvements in temperature

simulations. However, further downscaling through the nested domain seems to be problematic, enhancing biases over some regions. In general, the D2 simulation tends to produce higher temperatures than that of the D1 simulation. While certain regions showing cold bias are benefited, broader regions, particularly those characterized by high urban density, suffer from the overestimation of temperatures. It is noteworthy that CMFD observational patterns may not fully reflect the localized heat island effect over urban areas as CMFD is interpolated and regridded from a relatively sparse network of stations (He et al., 2020). This limitation may potentially exaggerate the warm bias over highly urbanized areas. However, the implementation of BEM is shown to alleviate this problem because the effect of BEM emerges in the direction of lowering the temperatures in urban areas. The difference between D2 simulations with and without BEM makes it clear that the regions having an urban density above 5% (Fig. 1 d, e) are roughly congruent with the counterparts where the D2 simulation with BEM yields a lower temperature. Interestingly, Tmax and Tmin responses to BEM emerge in a very different manner. While BEM aids in lowering Tmin, its impact on Tmax remains marginal. The asymmetric behavior between Tmax and Tmin may affect the diurnal variation of temperatures. Such responses of BEM within RegCM4-NH are mostly consistent with the findings presented by Oleson and Feddema (2020).

To uncover the main factors controlling temperature simulation, Fig. 4 presents the difference in net radiation ($\overrightarrow{S} - \overrightarrow{L}$), the sum of sensible and latent heat ($Q_H + Q_E$), and the difference in anthropogenic heat and net storage heat ($Q_F - Q_S$) between D2 simulations with and without BEM. BEM does not seem to make any significant change in the net radiation. Meanwhile, the spatial distribution of $Q_F - Q_S$ is highly correlated to the temperature difference illustrated in Fig. 3. Since the net storage heat flux ($Q_S$), which is a residual from the updated fluxes, should be small, it would be reasonable to infer that the values presented in Fig. 4 (c) mostly correspond to $Q_F$. This implies that BEM results in the reduction of anthropogenic heat ($Q_F$) over the urban area and that its magnitude is proportional to the urban density. Recalling the energy balance Eq. (1), the changes in turbulent heat fluxes is attributed to anthropogenic heat, which subsequently modulates the temperature.

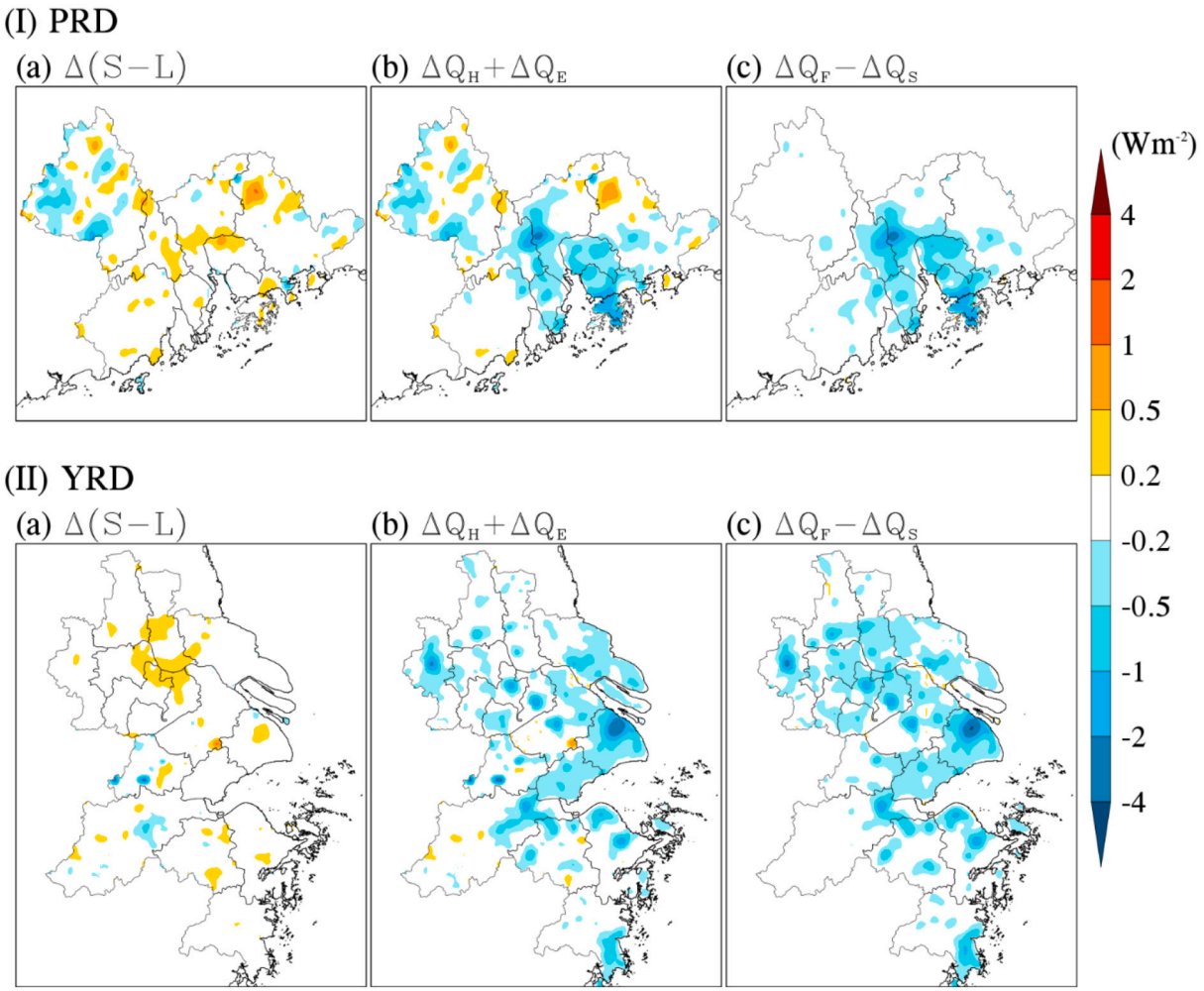


**Fig. 4.** The spatial distribution of 10-year average (2000–2009) JJA mean difference of net radiation flux (Δ(S – L)) (a), sensible and latent heat fluxes ($\Delta Q_H + \Delta Q_E$) (b), and anthropogenic and net storage heat fluxes ($\Delta Q_F - \Delta Q_S$) (c) (unit: $Wm^{-2}$) between the two nested domain simulations with and without BEM (D2-New - D2-Def) over PRD (I) and YRD (II).

To better understand the characteristics of temperature bias patterns, Fig. 5 presents the diurnal variation of temperature biases over the PRD and YRD regions from the D1 simulation and D2 simulations with default CLMU and with BEM every 3-hour. For both PRD and YRD regions, the D1 simulation shows the systematic cold bias throughout the whole day. The D2 simulations lead to a significant reduction of cold bias and their improvement is evident, particularly during the nighttime (e.g., 20LST, 23 LST, and 02LST) with a very small magnitude of bias. However, for the daytime (e.g., 11LST, 14LST, and 17 LST) over the YRD region, the magnitude of warm bias from both D2 simulations becomes larger than the cold bias seen in the D1 simulation, thereby revealing the skeptical aspect of nested simulation. The overestimation of temperature over the urban grids when the urban module turns on is not limited to our simulations but has already been reported in previous studies (Huszar et al., 2020a, 2020b). Although the BEM implementation does help reduce the temperature in comparison to D2 simulation with default CLMU during the nighttime, the positive benefit of BEM is seemingly not relevant. Even it is difficult to differentiate both D2 simulations in the daytime temperature. However, the bias calculated based on the climatological average could conceal the effect of BEM on a daily basis. Therefore, Fig. 5 also provides a fraction of the number of days whether the temperature at each time from the D2 simulation with default CLMU is higher or lower than the D2 simulation with BEM. Except for 14 LST and 17 LST over YRD, the D2 simulation with BEM produces many more days when the temperature is lower than that of the D2 simulation without BEM. Thus, the BEM seems to be able to help alleviate the well-known problem of the default CLMU that overestimates temperature over the urban grids.

### 3.2. Analysis of the effect of BEM depending on the urban density

For an in-depth analysis of how the effect of BEM emerges differently along different urban densities, three different categories (i.e., rural, suburban, and urban) are divided. While the rural area is defined if the total urban percentage is equal to or lower than 5% (shaded with gray and green in Fig. 1d & 1e), the suburban is defined if the total urban percentage is lower than 40% (shaded with orange and red in Fig. 1d & 1e). The study defines a region as urban if the total urban percentage is equal to or higher than 40% (shaded with dark purple in Fig. 1d & 1e). For the RegCM4-NH simulation with default CLMU, the urban land-use category was not assigned until its percentage reaches 40%. Such a stringent criterion reduces the urban area so that it could simply prevent the large contribution of high temperature from urban grids. For all experiments carried out in this study, the criterion is lowered to 5% to fully

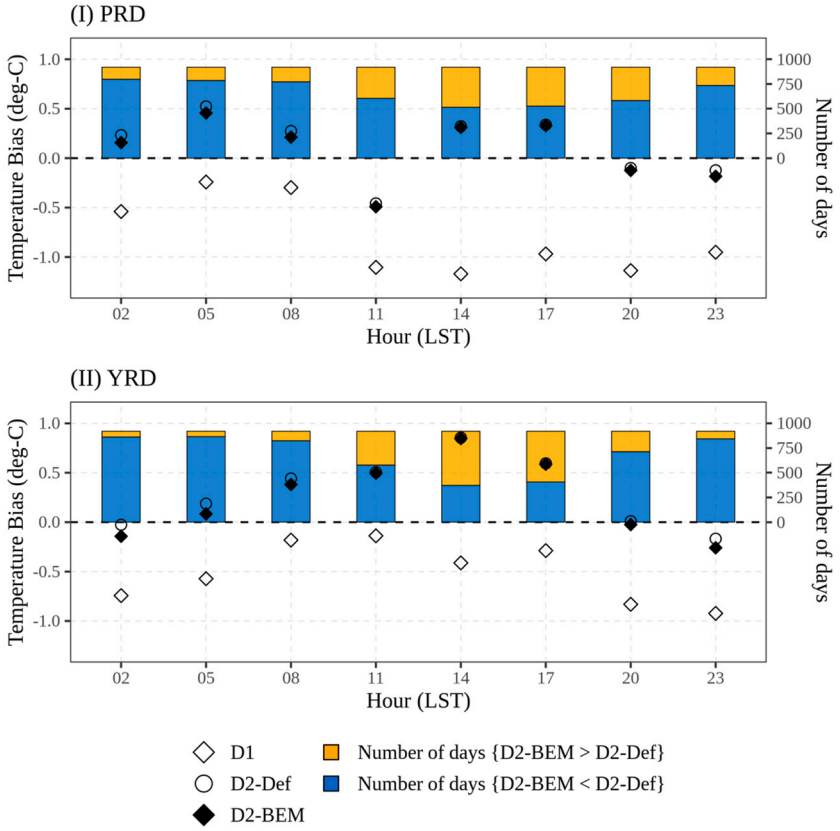


**Fig. 5.** The 10-year average of temperature biases simulated from D1 (open diamond), D2-Def (open circle), and D2-BEM (closed diamond) against CMFD observation for each local standard time (LST) over PRD (I) and YRD (II). The fractional colored bars present the number of days (totally 920 days) when the temperature from D2-BEM is warmer (orange) or cooler (blue) than that from D2-Def. (For interpretation of the references to colour in this figure legend, the reader is referred to the web version of this article.)

account for the urban effect. The topographical effect on temperature is eliminated to make a fair comparison of variables over regions with different urban densities. As seen in Fig. S2, the temperature climatology depicts a strong elevation dependency and the altitudinal displacement between rural and urban is quite different. While the majority of the urban grids are situated below 100 m, the rural grids exist in a much higher altitude. This may introduce the overestimation of the UHI effects which are normally estimated based on the temperature difference between rural and urban areas. Therefore, the temperatures are adjusted using the vertical gradient of the average lapse rate (i.e., 0.65 °C/100 m), which was also applied to the previous studies (Lowry, 1977; Martin-Vide et al., 2015; Ünal et al., 2020).

Fig. 6 presents the diurnal cycle of summer mean temperature over different urban categories (i.e., rural, suburban and urban). The boxplots at each local standard time (LST) provide some statistics of the spatial variability of temperature corresponding to each urban category. The most common feature appearing in both PRD and YRD regions is that all urban classes show the same timing of highest and lowest temperature at 14 LST and 05 LST, respectively, and that the temperatures from D2 simulations are systematically warmer than those from D1 simulation. For the PRD, D2 simulation is capable of making improvements in temperature across rural areas because D1 simulation shows a severe cold bias, particularly during the daytime. By contrast, D2 simulation tends to deteriorate temperature bias over the YRD rural area where D1 simulation already shows a warm bias. The positive impact of D2 simulation seemingly depends on the regions because the systematic bias of D1 simulation is different between YRD and PRD regions. On the other hand, the D2 simulation consistently overestimates temperature over suburban and urban areas where the CLMU is more active (Fig. 6b & 6c), regardless of the regions. This result reveals an obvious problem embedded in the urban module and the dataset of urban properties that are the same for China in its entirety. Meanwhile, the notable overestimations can partly be ascribed to observational undersampling across the areas with higher urban density. The boxplots for CMFD exhibit very small interquartile ranges in the urban (and even suburban) class, which shows that the resolution of CMFD is insufficient for capturing the localized urban effects. Implementation of BEM tends to slightly reduce the biases, especially during nighttime at higher density urban classes. However, the magnitude of this reduction may not be clearly visible from the climatological average pattern.

To understand how the BEM can produce different effects in the diurnal variation of temperature along the different urban

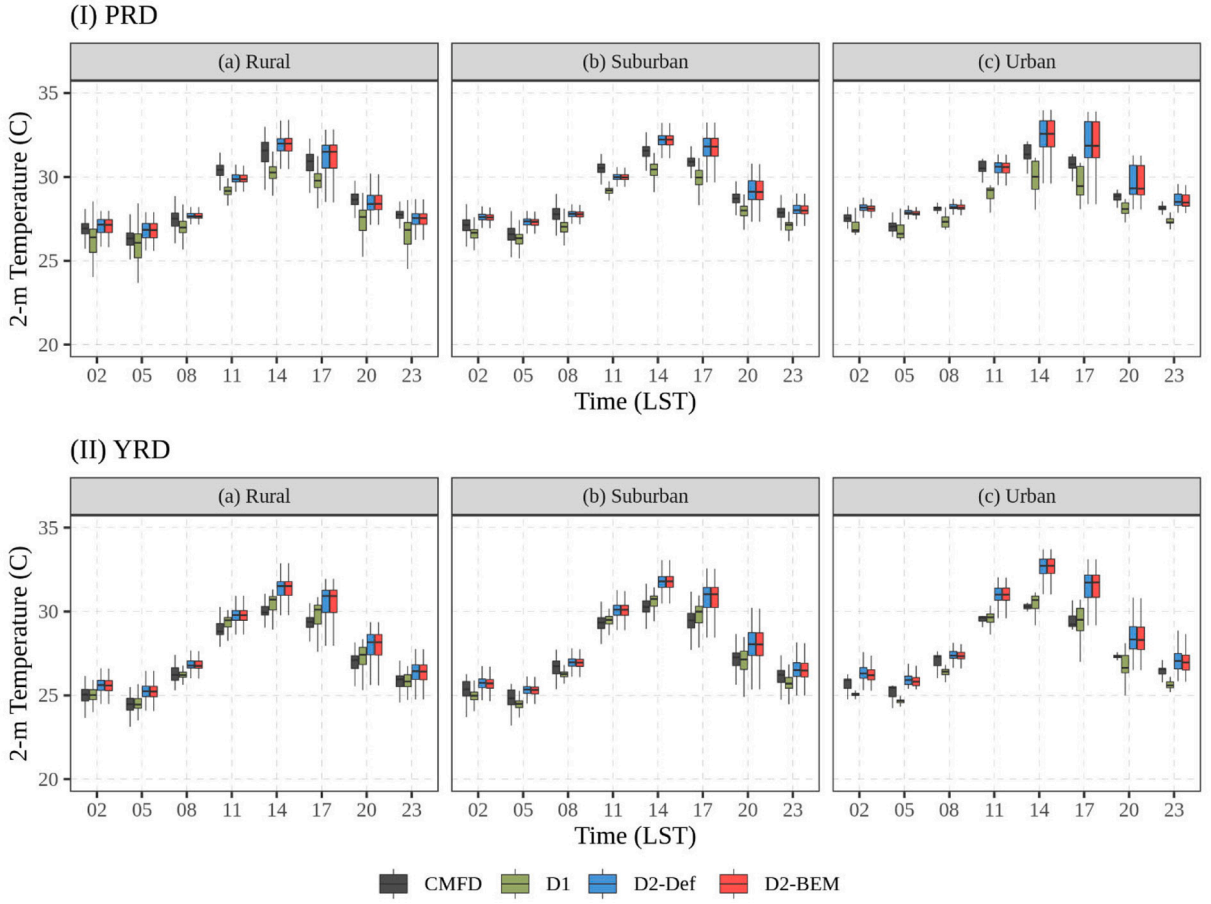


**Fig. 6.** Diurnal variation of 10-year average (2000–2009) JJA mean temperature over rural, suburban, and urban regions in PRD (I) and YRD (II) derived from CMFD observation, D1 simulation, and D2 simulations with and without BEM. The boxplot for each category (i.e., rural, suburban, and urban) is composed of the values from grid points with the altitude lower than 50 m corresponding to that region.

densities, Fig. 7 presents a diurnal variation of the difference in AHF and net storage heat flux ($Q_F - Q_S$) between D2 simulations with and without BEM. The effect of BEM emerges proportionally to urban density. The BEM can lead to the modification of the AHF that varies diurnally in urban areas, as opposed to almost no difference between the two simulations in rural areas. In particular, the BEM tends to release far less amount of AHF during the nighttime in the areas where urban density exceeds 40%. According to the formula (Eq. (3)), it may be attributed to the ventilation effect. The direction of heat transfer by ventilation depends on the sign of ($T_{iB} - T_{ac}$). During the nighttime, the ventilation may transfer more heat from the building to the outside and lower the air temperature inside the building (i.e., $T_{iB}$), thereby leading to the reduction of anthropogenic heat released from the air-conditioner. The opposite happens during the peak timing in $T_{ac}$, but its magnitude is marginal. The current formula considers the ventilation rate to be a single constant for the entire day. A more accurate rating of ventilation is expected to bring further improvements in the simulation.

For a more detailed analysis, the difference in temperature and heat fluxes between simulations with and without BEM is compared at the time of highest temperature (14 LST) and lowest temperature (05 LST) in the diurnal cycle. Fig. 8 presents the box plots of the differences between suburban and urban regions at 14 LST and at 05 LST. The difference is calculated at the daily time scales because the climatological mean may conceal the effect of BEM. Regarding temperature, the reason underlying the marginal effect in the daytime is attributed to the co-existence of a similar amount of positive and negative differences, positioning the median near zero. On the other hand, if the BEM is implemented, far more days produce lower temperatures at nighttime. The sum of sensible and latent heat fluxes exhibits a similar behavior seen in temperature, but the difference between daytime and nighttime becomes much clearer. The reduction of heat fluxes is balanced with the reduction of AHF, thus lowering the temperature. The temperature changes and related heat fluxes introduced by the implementation of BEM are consistent with the result presented in Oleson and Feddema (2020).

### 3.3. Comparative assessment of the UHI effect over the PRD and YRD regions

While Sections 3.1 and 3.2 focus on comparing two simulations with and without BEM to understand how the inclusion of BEM

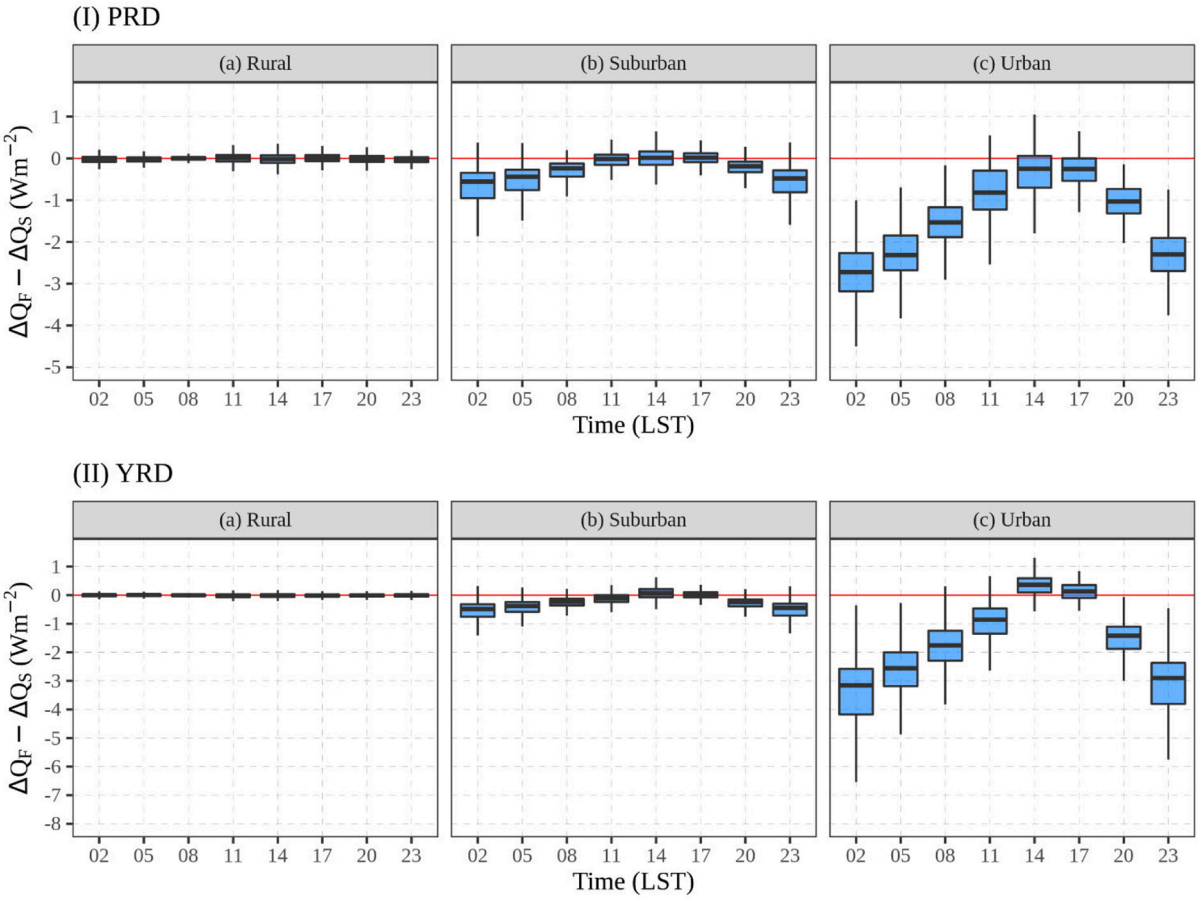


**Fig. 7.** Diurnal variation of 10-year average (2000–2009) JJA mean difference of anthropogenic and net storage heat fluxes ($\Delta Q_F - \Delta Q_S$) between the two nested domain simulations with and without BEM (D2-BEM minus D2-Def) over rural, suburban, and urban regions in PRD (I) and YRD (II). The boxplot for each category (i.e., rural, suburban, and urban) is composed of the values from grid points with the altitude lower than 50 m corresponding to that region.

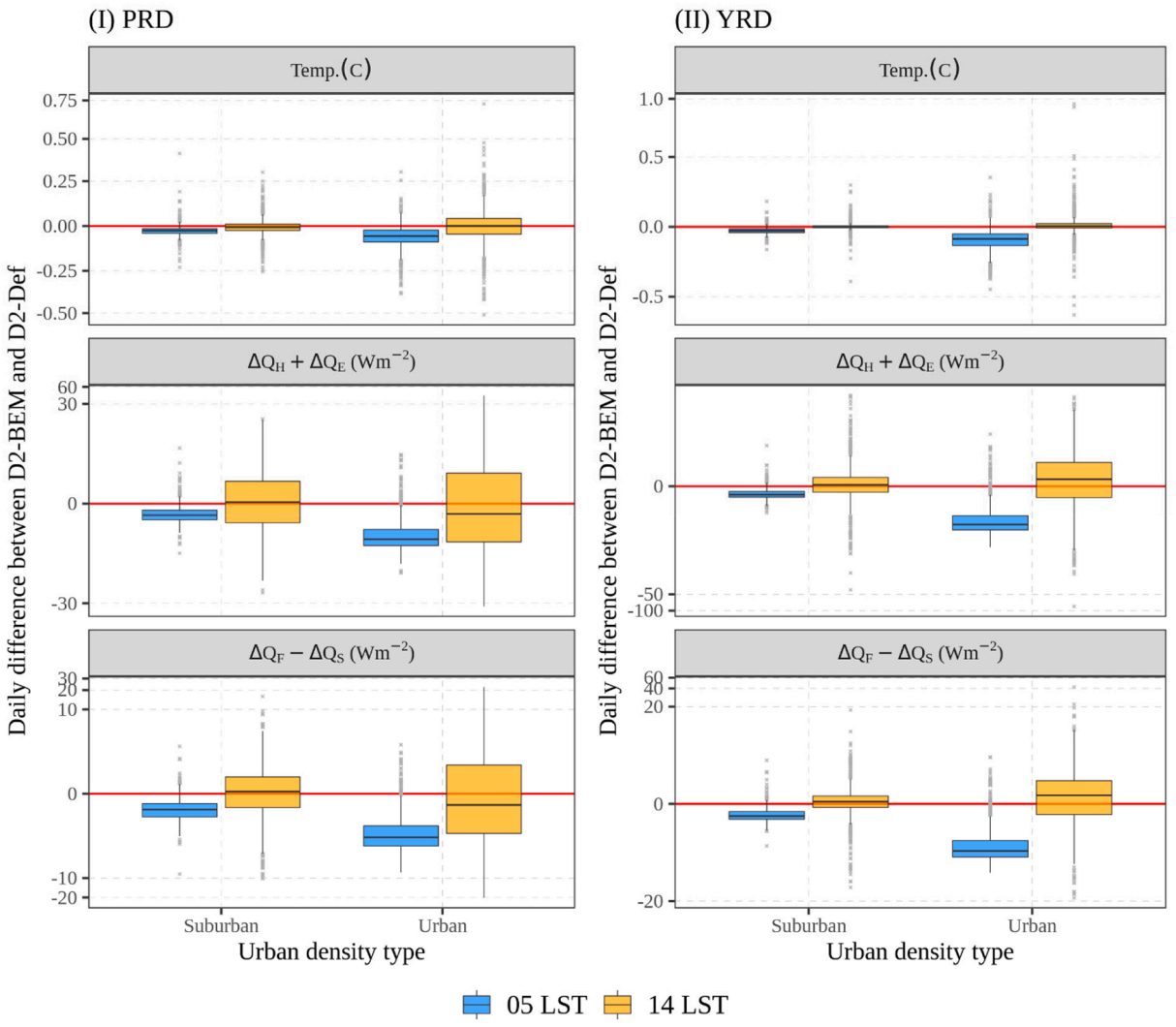


**Fig. 8.** Boxplot of daily differences (D2-BEM minus D2-Def) of temperature (upper, unit: °C), total sensible and latent heat fluxes (middle, unit: $Wm^{-2}$), and anthropogenic minus net storage heat fluxes (lower, unit: $Wm^{-2}$) at 05 LST and 14 LST over suburban and urban regions in PRD (I) and YRD (II) during the summer (JJA) of 10-year (2000–2009). The y-axis is transformed by "asinh" function (nearly same as log10, except it can be applied for zero and negative values) for better visualization.

leads to changes in the surface energy balance and resultant temperature, this section describes the urban heat island (UHI) effect calculated from the simulation with BEM. The UHI is an important indicator to characterize the urban climate and the feasibility of capturing it can exemplify the skill of RegCM4-NH with BEM as a modeling tool to be used for studying future urban expansion scenarios across the PRD and YRD regions. Here, the UHI is defined as the temperature difference between urban and rural (urban minus rural), which is the most well-known method (Yan et al., 2016; Zhao and Wu, 2017; Shi et al., 2019). Importantly, the intensity of UHI is sensitive to the selection of surrounding rural areas as a reference (Martin-Vide et al., 2015; Yan et al., 2016). Therefore, we apply the inverse distance weighting (IDW, Shepard, 1968) for the temperature difference between urban grid points and their surrounding lower urban density grid points, rather than confining the rural areas to specific grid points. Specifically, for each urban grid point "*i*", the $UHI_i$ is calculated as follows:

$$UHI_i = \frac{\sum_{r=1}^{r=n}\left[\frac{\left(T_{adjusted,i} - T_{adjusted,r}\right)}{\left(D_{ir}^2\right)}\right]}{\sum_{r=1}^{r=n}\left[\frac{1}{\left(D_{ir}^2\right)}\right]} \tag{4}$$

In Eq. (4), the temperature is firstly adjusted by elevation for all grid points. "***n***" denotes the number of surrounding lower density grid points "***r***", and "*D*" is the distance (in km) between "*i*" to each of "***r***".

Fig. 9 presents the spatial distribution of climatological UHI over the PRD and YRD regions at each LST. The geographical locations

of maximum UHI are in accordance with the urban density presented in Fig. 1. More significantly, a pronounced diurnal variation is observed in the development of UHI in both regions. The UHI tends to develop gradually through the morning and early afternoon. The maximum UHI in terms of intensity and extent then occurs in the late afternoon and evening (17 LST and 20 LST). This implies that the UHI exhibits a delayed response to temperature diurnal variation because daily maximum temperature usually occurs before the occurrence of maximum UHI. Such a time lag can be explained by the accumulation of the massive release of AHF during the daytime. The intensity of UHI weakens gradually with an increase in radiative cooling. The spatial and temporal variations of UHI seen in our simulation are qualitatively similar to the previous findings of Li et al. (2017).

Fig. 10 also investigates the relationship between the intensity of UHI and the background temperature. The analysis is performed at a daily timescale for 17 LST (a) and 20 LST (b) when the intensity of UHI is generally high over the studied domains. At each time, the UHI intensity and temperature anomaly from 10-year climatology are first computed with respect to individual grid points, before

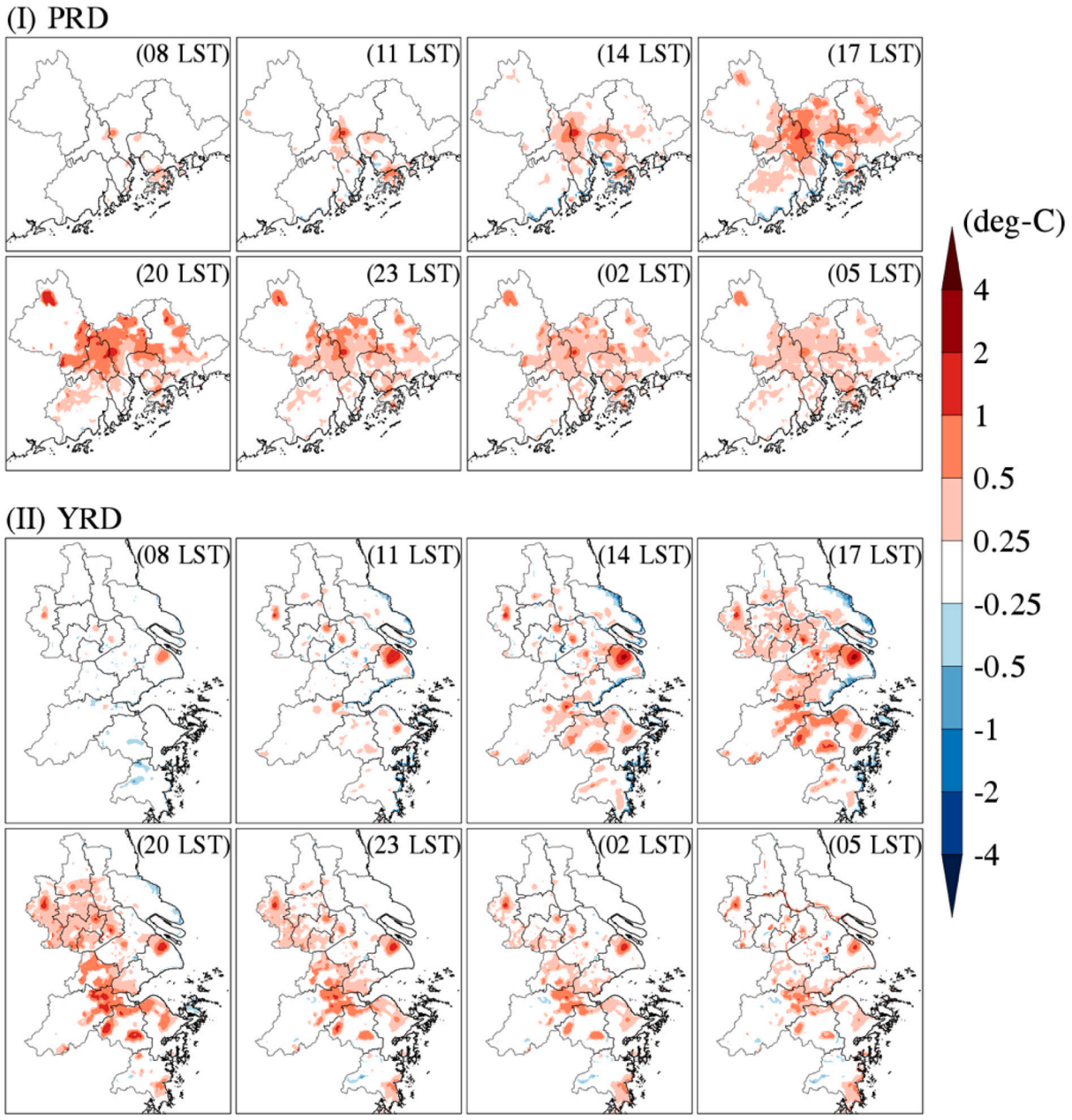


**Fig. 9.** The 10-year (2000–2009) climatology of spatial distribution of urban heat island effect (unit: °C) at each LST calculated from the inverse distance weighting for the difference of near-surface temperature between urban grid point and its surrounding grid points with lower urban density.

being area-averaged for urban and suburban areas to figure out the variation and dependence of UHI along with an anomalously warm day or a cool day at that time. Expectedly, the intensity of UHI is stronger in urban than in suburban for both PRD and YRD regions. However, the discrepancy between urban and suburban is much greater in YRD than in PRD. The YRD, which is situated at a relatively higher latitude in comparison to PRD, is characterized by a large variability range of temperature and UHI intensity. More importantly, the higher intensity of UHI tends to appear on anomalously hot days, thereby forming a strong correlation between UHI intensity and temperature anomaly. It is reasonable to envision dangerous levels of heat stress on anomalous hot days in YRD in summer. Furthermore, adding approximately 1–2° higher temperature due to UHI may exacerbate the risk level to extremely intolerable circumstances, particularly for the urban population exposed to poor living conditions. The positive correlation between temperature anomaly and UHI intensity becomes stronger at 20 LST for PRD and at 17 LST for YRD, which are in line with the peak timing in UHI diurnal variation illustrated in Fig. 9. Given that some previous studies have shown that urban expansion may contribute to the warming trend (Lin et al., 2016; Shi et al., 2019), it is crucial to ascertain how this positive correlation will evolve and affect extreme heat stress in a warmer climate, which will be explored in our future work.

## 4. Summary and discussion

In this study, the BEM introduced by Oleson and Feddema (2020) was incorporated into CLMU in RegCM4-NH to alleviate the severe overestimation of temperature in urban grids which is a well-known bias reported by other studies based on the high-resolution RegCM4 simulations (e.g., Huszar et al., 2020a, 2020b). The urban distribution and properties are also updated in both simulations with and without BEM using the urban dataset provided by Oleson and Feddema (2020) from the one provided by Jackson et al. (2010). Currently, the default set-up of RegCM4-NH does not account for low-to-medium density urban and CLMU only works for the

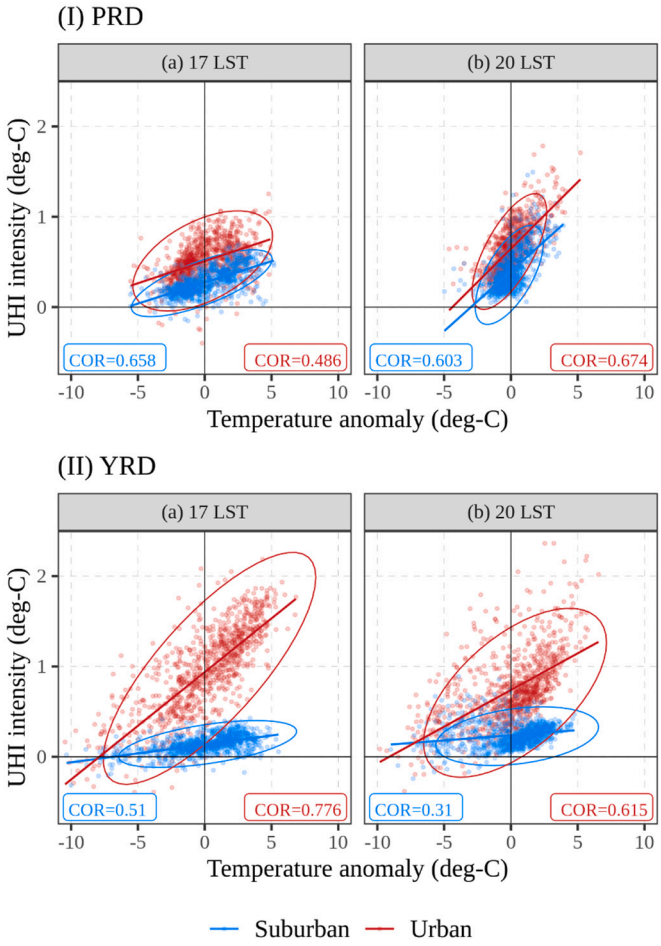


**Fig. 10.** Scatterplot for the relationship between UHI intensity (unit: °C) and near-surface temperature anomaly (unit: °C) averaged over urban and suburban in PRD and YRD at 17 LST (a) and 20 LST (b) during the summer (JJA) of 10-year (2000–2009). For each urban category, the ellipse is based on the multivariate t-distribution at 0.99 level while the line is from a simple linear regression considering UHI intensity as function of near-surface temperature anomaly. For each panel, the Spearman's correlation coefficients between the two variables are shown in the bottom-left and bottom-right corners for suburban and urban, respectively.

grids where the urban fraction is over 40% so that the overestimation bias in urban grids may be less apparent. In this regard, the evaluation of the RegCM4-NH with BEM in simulating urban climate at very high resolution (i.e. 4 km) can serve as a benchmark for future use by the RegCM community. In addition, since most previous studies focusing on the urbanization effect based on the RegCM modeling system have been limited to the European region, our simulations targeted on the PRD and YRD regions will provide pertinent insights into the transferability of the RegCM-NH to other urban agglomerations for the purpose of studying the urban effect on regional climate.

A significant body of studies has demonstrated that the emission of AHF from the buildings plays a crucial role in simulating the urban climate (Sailor, 2011; Chrysoulakis and Grimmond, 2016; Zhang et al., 2016; Wang et al., 2019), thus emphasizing the importance of a realistic representation of the processes related to the building in the urban model. Although the role of the urban model has not been seriously considered for the hydrostatic version of RegCM4, the release of and transition to RegCM4-NH may underscore the need to improve the urban canopy model in RegCM4-NH. In this regard, the implementation of BEM and the demonstration of physical realism expected from the BEM could indeed be valuable. The comparison of two simulations with and without BEM reveals that the effect of BEM emerges in the form of a slight reduction of the nocturnal warm bias, whereas the severe overestimation of daytime temperature mostly remains unchanged. Compared to the default CLMU, the BEM treats the interior building temperature ($T_{iB}$) as a prognostic variable updating every time step while also taking into consideration the ventilation and heat transfer between the building and the ground. Obviously, the calculation procedure of $T_{iB}$ is more comprehensive in BEM than in default CLMU, and therefore it is reasonable to expect that $T_{iB}$ derived from BEM can positively impact model performance. The accuracy of $T_{iB}$ is essential to determine the amount of heat removed and/or wasteheat as the AHF is released into the atmosphere, which contributes to the energy balance in the urban canopy. In our simulation, the BEM brings the systematic reduction of AHF during the night, leading to a decrease in temperature. Apart from the improvement by adding BEM, this study demonstrates that the RegCM4-NH with the BEM is capable of reasonably capturing the relevant patterns of UHI effect over the PRD and YRD regions, which are commonly observed in other regions (Zhang et al., 2010; Zhang et al., 2016; Li et al., 2017; Lin et al., 2016; Shi et al., 2019). The experimental design with two nested domains corresponding to the PRD and YRD (See Fig. 1) offers a unique opportunity to address the role of background climate on the effect of UHI. The positive relationship between the intensity of UHI and temperature anomaly is more obvious in YRD than in PRD, indicating the region-specific impacts of urbanization. These findings could serve as a benchmark before conducting the future climate projections to understand the climate impact of future urban growth in a warmer climate. Furthermore, the modeling skill exemplified by RegCM4-NH with the BEM could have significant implications for the RegCM4 community.

Despite an encouraging result, we are aware of critical limitations and the fact that there is significant room for further improvement. First, the lack of detailed property data of building for each domain impedes the efforts to further fine-tune this model. This includes not only the problem of sharing similar urban features in PRD and YRD, but also omitting some key processes. Second, the diurnal variation of ventilation, which is assigned as a single constant, could also be an important factor to improve the model accuracy. As a case in point, the findings from Wang et al. (2019) suggest that a more realistic estimation of ventilation could be achieved by using the instantaneous indoor $CO_2$ concentration. The contribution of vehicles emission and another major source of anthropogenic heat should also be considered in the model. Although CLMU has already provided a very simple estimation for traffic activities, this module is disabled in RegCM4-NH and requires further investigation before it can be used properly. In addition, long-term climate simulations should be performed with the regular change of urban expansion because the transition from agriculture or grassland to urban structures has shown crucial roles in modifying local climate (Doan et al., 2016; Doan and Kusaka, 2016). Inevitably, these improvements can only be implemented with the more detailed and realistic information of the urban at finer scale resolution.

## Author contributions

E.-S. IM and T. Nguyen-Xuan conceived this study. T. Nguyen-Xuan developed the code under the supervision of E.-S. IM. Both authors discussed the results and wrote the manuscript.

## Declaration of Competing Interest

The authors declare that the research was conducted in the absence of any commercial or financial relationships that could be construed as a potential conflict of interest.

## Data availability

The data that support the findings of this study are available from the corresponding author upon reasonable request.

## Acknowledgements

This study was supported by the Hong Kong Research Grants Council funded project (ECS26309618). The authors would like to thank the Earth System Physics team at Abdus Salam International Centre for Theoretical Physics for providing the valuable comments and technical support in using the non-hydrostatic version of RegCM4. The authors also extend their gratitude to the HKUST Fok Ying Tung Research Institute and National Supercomputing Center in Guangzhou Nansha Sub-center for providing high performance computational resources.

## Appendix A. Supplementary data

Supplementary data to this article can be found online at https://doi.org/10.1016/j.uclim.2023.101527.

## References


Ban, N., Caillaud, C., Coppola, E., et al., 2021. The first multi-model ensemble of regional climate simulations at kilometer scale resolution, part I: evaluation of precipitation. Clim. Dyn. https://doi.org/10.1007/s00382-021-05708-w.

Bueno, B., Pigeon, G., Norford, L.K., Zibouche, K., Marchadier, C., 2012. Development and evaluation of a building energy model integrated in the TEB scheme. Geosci. Model Dev. 5, 433–448. https://doi.org/10.5194/gmd-5-433-2012.

Chen, F., Kusaka, H., Bornstein, R., Ching, J., Grimmond, C.S.B., Grossman-Clarke, S., Loridan, T., Manning, K.W., Martilli, A., Miao, S., Sailor, D., Salamanca, F.P., Taha, H., Tewari, M., Wang, X., Wyszogrodzki, A.A., Zhang, C., 2011. The integrated WRF/urban modelling system: development, evaluation, and applications to urban environmental problems. Int. J. Climatol. 31, 273–288. https://doi.org/10.1002/joc.2158.

Chrysoulakis, N., Grimmond, C.S.B., 2016. Understanding and reducing the anthropogenic heat emission. In: Santamouris, M., Kolokotsa, D. (Eds.), Urban Climate Mitigation Techniques. Routledge, pp. 27–40. ISBN 9780415712132.

Coppola, E., Sobolowski, S., Pichelli, E., et al., 2020. A first-of-its-kind multi-model convection permitting ensemble for investigating convective phenomena over Europe and the Mediterranean. Clim. Dyn. 55, 3–34. https://doi.org/10.1007/s00382-018-4521-8.

Coppola, E., Stocchi, P., Pichelli, E., Torres Alavez, J.A., Glazer, R., Giuliani, G., Di Sante, F., Nogherotto, R., Giorgi, F., 2021. Non-hydrostatic RegCM4 (RegCM4-NH): model description and case studies over multiple domains. Geosci. Model Dev. Discuss. https://doi.org/10.5194/gmd-2020-435 [preprint].

Dai, J., Wang, X., Dai, W., Chang, M., 2019. The impact of inhomogeneous urban canopy parameters on meteorological conditions and implications for air quality in the Pearl River Delta region. Urban Clim. 29, 100494 https://doi.org/10.1016/j.uclim.2019.100494.

Dee, D.P., Uppala, S.M., Simmons, A.J., Berrisford, P., Poli, P., Kobayashi, et al., 2011. The ERA-interim reanalysis: configuration and performance of the data assimilation system. Q. J. R. Meteorol. Soc. 137 (656), 553–597. https://doi.org/10.1002/qj.828.

Doan, Q.-V., Kusaka, H., 2016. Numerical study on regional climate change due to the rapid urbanization of greater Ho Chi Minh City's metropolitan area over the past 20 years. Int. J. Climatol. 36 (10), 3633–3650. https://doi.org/10.1002/joc.4582.

Doan, Q.-V., Kusaka, H., Ho, Q.-B., 2016. Impact of future urbanization on temperature and thermal comfort index in a developing tropical city: Ho Chi Minh City. Urban Clim. 17, 20–31. https://doi.org/10.1016/j.uclim.2016.04.003.

Doan, Q.-V., Kusaka, H., Nguyen-Minh, T., 2019. Roles of past, present, and future land use and anthropogenic heat release changes on urban heat island effects in Hanoi, Vietnam: numerical experiments with a regional climate model. Sustain. Cities Soc. 47, 101479 https://doi.org/10.1016/j.scs.2019.101479.

Emanuel, K.A., Živković-Rothman, M., 1999. Development and evaluation of a convection scheme for use in climate models. J. Atmos. Sci. 56 (11), 1766–1782. https://doi.org/10.1175/1520-0469(1999)056<1766:DAEOAC>2.0.CO;2.

Feddema, J., Kauffman, B., 2016. Urban Properties Tool (Version 1.2). NCAR THESIS Tools Library. Retrieved from: https://svn-iam-thesis-release.cgd.ucar.edu/urban_properties/ https://doi.org/10.5065/D6R78CMT.

Giorgi, F., Coppola, E., Solmon, F., et al., 2012. RegCM4: model description and preliminary tests over multiple CORDEX domains. Clim. Res. 52, 31–48.

Grimmond, C.S.B., et al., 2009. Urban surface energy balance models: model characteristics and methodology for a comparison study. In: Baklanov, A., et al. (Eds.), Meteorological and Air Quality Models for Urban Areas. https://doi.org/10.1007/978-3-642-00298-4_11.

Grimmond, C.S.B., et al., 2011. Initial results from phase 2 of the international urban energy balance model comparison. Int. J. Climatol. 31 (2), 244–272. https://doi.org/10.1002/joc.2227.

Halenka, T., Belda, M., Huszar, P., Karlicky, J., Novakova, T., Zak, M., 2019. On the comparison of urban canopy effects parameterisation. Int. J. Environ. Pollut. 65 (1/2/3), 177–194.

He, J., Yang, K., Tang, W., Lu, H., Qin, J., Chen, Y.Y., Li, X., 2020. The first high-resolution meteorological forcing dataset for land process studies over China. Sci. Data 7 (25). https://doi.org/10.1038/s41597-020-0369-y.

Holtslag, A., Bruijn, E.D., Pan, H., 1990. A high resolution air mass transformation model for short-range weather forecasting. Mon. Weather Rev. 118, 1561–1575.

Huszar, P., Karlický, J., Ďoubalová, J., Šindelářová, K., Nováková, T., Belda, M., Halenka, T., Žák, M., Pišoft, P., 2020a. Urban canopy meteorological forcing and its impact on ozone and PM2.5: role of vertical turbulent transport. Atmos. Chem. Phys. 20, 1977–2016. https://doi.org/10.5194/acp-20-1977-2020.

Huszar, P., Karlický, J., Ďoubalová, J., Nováková, T., Šindelářová, K., Švábik, F., Belda, M., Blouse, T., Žák, M., 2020b. The impact of urban land-surface on extreme air pollution over Central Europe. Atmos. Chem. Phys. 20, 11655–11681. https://doi.org/10.5194/acp-20-11655-2020.

Jackson, T., Feddema, J., Oleson, K., Bonan, G., Bauer, J., 2010. Parameterization of urban characteristics for global climate modeling. Ann. Assoc. Am. Geogr. 100 (4), 848–865. http://www.jstor.org/stable/40863606.

Karlický, J., Huszár, P., Halenka, T., Belda, M., Žák, M., Pišoft, P., Mikšovský, J., 2018. Multi-model comparison of urban heat island modelling approaches. Atmos. Chem. Phys. 18, 10655–10674. https://doi.org/10.5194/acp-18-10655-2018.

Karlický, J., Huszár, P., Nováková, T., Belda, M., Švábik, F., Ďoubalová, J., Halenka, T., 2020. The "urban meteorology island": a multi-model ensemble analysis. Atmos. Chem. Phys. 20, 15061–15077. https://doi.org/10.5194/acp-20-15061-2020.

Kiehl, J., Hack, J., Bonan, G., Boville, B., Williamson, D., Rasch, P., 1998. The National Center for Atmospheric Research Community climate model: CCM3. J. Clim. 11, 1131–1149.

Kwok, Y.T., Ng, E.Y.Y., 2021. Trends, topics, and lessons learnt from real case studies using mesoscale atmospheric models for urban climate application in 2000-2019. Urban Clim. 36, 100785 https://doi.org/10.1016/j.uclim.2021.100785.

Li, M., Wang, T., Xie, M., et al., 2017. Modeling of urban heat island and its impacts on thermal circulations in the Beijing–Tianjin–Hebei region, China. Theor. Appl. Climatol. 128, 999–1013. https://doi.org/10.1007/s00704-016-1903-x.

Lin, S., Feng, J., Wang, J., Hu, Y., 2016. Modeling the contribution of long-term urbanization to temperature increase in three extensive urban agglomerations in China. J. Geophys. Res. Atmos. 121, 1683–1697. https://doi.org/10.1002/2015JD024227.

Lowry, W., 1977. Empirical estimation of urban effects on climate: a problem analysis. J. Appl. Meteorol. 16, 129–135.

Martin-Vide, J., Sarricolea, P., Moreno-García, M.C., 2015. On the definition of urban heat island intensity: the "rural" reference. Front. Earth Sci. 3, 24. https://doi.org/10.3389/feart.2015.00024.

Nguyen-Xuan, T., Lam, S.L., Giorgi, F., et al., 2021. Evaluation of the performance of the non-hydrostatic RegCM4 (RegCM4-NH) over southeastern China. Clim. Dyn. https://doi.org/10.1007/s00382-021-05969-5.

Oleson, K., 2012. Contrasts between urban and rural climate in CCSM4 CMIP5 climate change scenarios. J. Clim. 25 (5), 1390–1412.

Oleson, K.W., Feddema, J., 2020. Parameterization and surface data improvements and new capabilities for the community land model urban (CLMU). J. Adv. Model. Earth Syst. 12 https://doi.org/10.1029/2018MS001586 e2018MS001586.

Oleson, K.W., Lawrence, D.M., 2013. Technical description of version 4.5 of the community land model (CLM). In: NCAR Technical Note NCAR/TN-503+STR. NCAR, Boulder, CO, USA.

Oleson, K.W., Bonan, G.B., Feddema, J., Vertenstein, M., Grimmond, C.S.B., 2008a. An urban parameterization for a global climate model. Part I: formulation and evaluation for two cities. J. Appl. Meteorol. Climatol. 47, 1038–1060. https://doi.org/10.1175/2007jamc1597.1.

Oleson, K.W., Bonan, G.B., Feddema, J., Vertenstein, M., 2008b. An urban parameterization for a global climate model. Part II: sensitivity to input parameters and the simulated urban heat island in offline simulations. J. Appl. Meteorol. Climatol. 47, 1061–1076. https://doi.org/10.1175/2007jamc1598.1.

Pal, J.S., Small, E.E., Eltahir, E.A.B., 2000. Simulation of regional-scale water and energy budgets: representation of subgrid cloud and precipitation processes within RegCM. J. Geophys. Res. 105 (D24), 29579–29594.
Pichelli, E., Coppola, E., Sobolowski, S., et al., 2021. The first multi-model ensemble of regional climate simulations at kilometer-scale resolution part 2: historical and future simulations of precipitation. Clim. Dyn. https://doi.org/10.1007/s00382-021-05657-4.
Qing, Y., Wang, S., 2021. Multi-decadal convection-permitting climate projections for China's Greater Bay Area and surroundings. Clim. Dyn. 57, 415–434. https://doi.org/10.1007/s00382-021-05716-w.
Sailor, D.J., 2011. A review of methods for estimating anthropogenic heat and moisture emissions in the urban environment. Int. J. Climatol. 31, 189–199. https://doi.org/10.1002/joc.2106.
Shepard, D., 1968. A two-dimensional interpolation function for irregularly-spaced data. In: Association for Computing Machinery, Proceeding of the 1968 23rd ACM national Conference, pp. 517–524. https://doi.org/10.1145/800186.810616.
Shi, Z., Jia, G., Hu, Y., et al., 2019. The contribution of intensified urbanization effects on surface warming trends in China. Theor. Appl. Climatol. 138, 1125–1137. https://doi.org/10.1007/s00704-019-02892-y.
Ünal, Y.S., Sonuç, C.Y., Incecik, S., et al., 2020. Investigating urban heat island intensity in Istanbul. Theor. Appl. Climatol. 139, 175–190. https://doi.org/10.1007/s00704-019-02953-2.
United Nations, Department of Economic and Social Affairs, Population Division, 2018. World Urbanization Prospects: The 2018 Revision, Online Edition.
Wang, J., Feng, J., Yan, Z., Hu, Y., Jia, G., 2012. Nested high-resolution modeling of the impact of urbanization on regional climate in three vast urban agglomerations in China. J. Geophys. Res. 177, D21103. https://doi.org/10.1029/2012JD018226.
Wang, Y.-C., Bian, Z.-F., Qin, K., Zhang, Y., Lei, S.-G., 2019. A modified building energy model coupled with urban parameterization for estimating anthropogenic heat in urban areas. Energy & Build. 202, 109377 https://doi.org/10.1016/j.enbuild.2019.109377.
Wang, Z., Xiao, Z., Tam, C.-Y., Pan, W., Chen, J., et al., 2021. The projected effects of urbanization and climate change on summer thermal environment in Guangdong-Hong Kong-Macao Greater Bay Area of China. Urban Clim. 37, 100866 https://doi.org/10.1016/j.uclim.2021.100866.
Wong, N.H., He, Y., Nguyen, N.S., Raghavan, S.V., Martin, M., Hii, D.J.C., Yu, Z., Deng, J., 2021. An integrated multiscale urban microclimate model for urban thermal environment. Urban Clim. 35, 100730 https://doi.org/10.1016/j.uclim.2020.100730.
Xiao, Z., Wang, Z., Pan, W., Wang, Y., Yang, S., 2019. Sensitivity of Extreme Temperature Events to Urbanization in the Pearl River Delta Region. Asia-Pacific J Atmos Sci 55, 373–386. https://doi.org/10.1007/s13143-018-0094-z.
Yan, Z.-W., Wang, J., Xia, J.-J., Feng, J.-M., 2016. Review of recent studies of the climatic effects of urbanization in China. Adv. Clim. Chang. Res. 7, 154–168. https://doi.org/10.1016/j.accre.2016.09.003.
Yang, K., He, J., 2019. China Meteorological Forcing Dataset (1979-2018). National Tibetan Plateau Data Center. https://doi.org/10.11888/AtmosphericPhysics.tpe.249369.file.
Yang, B., Yang, X., Leung, L.R., Zhong, S., Qian, Y., Zhao, C., et al., 2019. Modeling the impacts ofurbanization on summer thermalcomfort: the role of urban land use andanthropogenic heat. J. Geophys. Res.-Atmos. 124, 6681–6697. https://doi.org/10.1029/2018JD029829.
Zeng, X., Zhao, M., Dickinson, R.E., 1998. Intercomparison of bulk aerodynamic algorithms for the computation of sea surface fluxes using TOGA COARE and TAO data. J. Clim. 11 (10), 2628–2644.
Zhang, N., Gao, Z., Wang, X., Chen, 2010. Modeling the impact of urbanization on the local and regional climate in Yangtze River Delta, China. Theor. Appl. Climatol. 102, 331–342. https://doi.org/10.1007/s00704-010-0263-1.
Zhang, N., Wang, X., Chen, Y., Dai, W., Wang, X., 2016. Numerical simulations on influence of urban land cover expansion and anthropogenic heat release on urban meteorological environment in Pearl River Delta. Theor. Appl. Climatol. 126, 469–479. https://doi.org/10.1007/s00704-015-1601-0.
Zhao, D., Wu, J., 2017. The influence of urban surface expansion in China on regional climate. J. Clim. 30 (3), 1060–1080. https://doi.org/10.1175/JCLI-D-15-0604.1.